NASA Technical Memorandum 110254

On Longitudinal Control of High Speed Aircraft in the Presence of Aeroelastic Modes

Suresh M. Joshi
NASA Langley Research Center, Hampton, Virginia

Atul G. Kelkar
Kansas State University, Manhattan, Kansas

May 1996

National Aeronautics and
Space Administration
Langley Research Center
Hampton, Virginia 23681-0001

Abstract

Longitudinal control system design is considered for a linearized dynamic model of a supersonic transport aircraft concept characterized by relaxed static stability and significant aeroelastic interactions. Two LQG-type controllers are designed using the frequency-domain additive uncertainty formulation to ensure robustness to unmodeled flexible modes. The first controller is based on a 4th-order model containing only the rigid-body modes, while the second controller is based on an 8th-order model that additionally includes the two most prominent flexible modes. The performance obtainable from the 4th-order controller is not adequate, while the 8th-order controller is found to provide better performance. Frequency-domain and time-domain (Lyapunov) methods are subsequently used to assess the robustness of the 8th-order controller to parametric uncertainties in the design model.

Summary

Longitudinal control system design is considered for a linearized dynamic model of a supersonic transport aircraft concept. The model consists of rigid-body modes and 18 aeroelastic modes. Two LQG-type controllers are designed using the frequency-domain additive uncertainty formulation to represent the unmodeled flexible modes. The first controller is based on a 4th-order model containing only the rigid-body modes, while the second controller is based on an 8th-order model that additionally includes the two most prominent flexible modes. Both controllers are designed to provide stability robustness in the presence of unmodeled flexible modes. The performance obtainable from the 4th-order design is not adequate. The 8th-order controller can provide better performance, although it cannot substantially improve the flexible mode damping ratios. Frequency-domain and time-domain (Lyapunov) methods are subsequently used to assess the robustness of the 8th-order controller to parametric uncertainties in the design model. The frequency-domain methods are found to give less conservative bounds on permissible parametric uncertainties than the time-domain methods, but are still overly conservative compared to the bounds obtained by numerical simulation. The results also indicate that a single actuator may not be sufficient to obtain higher controller performance, and underscore the need for further research on reducing the conservatism of Lyapunov-based methods.

1 Introduction

Large high-speed aircraft are characterized by static instability, low structural stiffness, and significant aeroelastic interactions. Furthermore, large parametric changes can occur over the flight envelope because of shifting of the center of gravity and aerodynamic center. In addition, the frequencies, damping ratios, and mode shapes of the aeroelastic modes are not known accurately. As a result, the problem of designing a control system which will maintain closed-loop stability and desired performance, is a challenging problem.

In this paper, we consider a mathematical model that is based on the supersonic cruise aircraft (SCRA) model developed in [1]. The SCRA concept is a delta wing supersonic aircraft which is nearly 300 ft. long and has a wing span of about 140 ft. The takeoff weight is 730,000 lbf, and the mid-cruise speed is Mach 2.3 at 53,000 ft. altitude. LQG-type control laws are designed to provide stability robustness in the presence of unmodeled flexible modes. The designs are based on two reduced-order mathematical models. The first model consists only of the rigid-body modes, while the second model additionally includes the two most prominent flexible modes. The robustness of the control system to parametric uncertainties in the design model is investigated using Lyapunov-based methods and frequency-domain methods.

2 Mathematical Model

We consider a linearized longitudinal model of the SCRA [1] in rectilinear wing-level ascent flight condition at weight 730,000 lbf, Mach 0.6, and 6,500 ft. altitude. This model was modified in [2] to reflect static instability that is present in recent high-speed civil transport (HSCT) concepts. The model is given by:

$$\dot{x}_f = A_f x_f + B_f u \tag{1}$$

where

$$x_f = (\xi, z, \theta, \overline{u}, \overline{w}, q, \eta^T, \dot{\eta}^T)^T \tag{2}$$

where ξ, z, denote the horizontal and vertical (rigid-body) center-of-mass (c.m.) positions and $\overline{u}, \overline{w}$ denote the corresponding velocities; θ and q denote the rigid-body pitch angle and rate; η is the 18×1 modal amplitude vector. A_f is the 42×42 system matrix, B_f is the 42×1 input matrix, and u denotes the elevator deflection.

The center of mass is located 2,364 in. from the front of the aircraft. Two pitch rate sensors (rate gyros), located at fore (2,050 in. from the front) and aft (2,500 in.) locations in reference to the center of mass, produce the 2×1 output vector $y(t)$ which consists of the contributions of q as well as $\dot{\eta}$.

The position variables ξ and z are ignorable and can be removed from (1), which results in the following 40th-order system

$$\dot{x} = Ax + Bu \tag{3}$$

$$y = Cx \tag{4}$$

where $x = (\theta, \overline{u}, \overline{w}, q, \eta^T, \dot{\eta}^T)^T$. The matrices A, B, and C have the following structures:

$$A = \begin{bmatrix} A_{11(4\times4)} & A_{12(4\times18)} & A_{13(4\times18)} \\ 0_{18\times4} & 0_{18\times18} & I_{18\times18} \\ A_{31(18\times4)} & A_{32(18\times18)} & A_{33(18\times18)} \end{bmatrix}$$

$$B = [0, 0, b_3, b_4, 0_{1\times18}, \Phi_{1\times18}]$$

$$C = \begin{bmatrix} 0_{1\times3} & 1 & 0_{1\times18} & \Psi_{1(1\times18)} \\ 0_{1\times3} & 1 & 0_{1\times18} & \Psi_{2(1\times18)} \end{bmatrix}$$

The first row of A_{11} is $(0, 0, 0, 1)$, while the first rows of A_{12} and A_{13} are zero. The matrices indicate strong dynamic coupling between the rigid and flexible modes, as well as significant contribution of the flexible modes to the sensed outputs.

The open-loop eigenvalues of A are shown in Table I. It can be seen that the rigid-body modes consist of two real eigenvalues, one positive and one negative, corresponding to the statically unstable short period mode, and a pair of stable complex eigenvalues

corresponding to a mid-period phugoid-like mode. The flexible mode frequencies range from 6.646 rad/sec for the first mode, to 47.298 rad/sec for the 18th mode. The damping ratios for the flexible modes range from 0.0139 to 0.1695, the average being 0.0462. The flexible modes are primarily fuselage bending modes. Modes 1 and 3 basically represent free fuselage bending modes (1st and 2nd), and Mode 2 is similar to the "cantilevered" fuselage 1st bending mode [2]. Mode 4 is similar to the 2nd cantilevered fuselage bending mode, and the shapes of the higher modes go up in complexity. The order of the mathematical model is 40; however, for practical implementation, it is desirable to design a reduced-order controller. In addition, the uncertainty in the model parameters is generally higher for higher frequency modes; hence it is desirable to avoid the use of higher mode parameters in control systems design. A reduced-order controller can be designed in two ways: 1) Design a full-order controller and then apply order reduction methods, or 2) Use a reduced-order design model. The second method is generally preferable because it does not rely on the knowledge of the higher-mode parameters, which is highly inaccurate.

3 Model Order Reduction

To investigate order reduction, a number of similarity transformations were performed. First, the A matrix was transformed to a quasi-diagonal form wherein the real eigenvalues appear on the diagonal, and the remaining 2×2 blocks correspond to the complex eigenvalue pairs ($\sigma_i \pm j\omega_i$). The next transformation rearranged the diagonal blocks of the A matrix so that the rigid-body eigenvalues appear in the first 4×4 diagonal block and the 2×2 blocks for the flexible modes appear in ascending order of natural frequencies:

$$A = \begin{bmatrix} \Lambda & 0 & . & . & 0 \\ 0 & \begin{bmatrix} \sigma_1 & \omega_1 \\ -\omega_1 & \sigma_1 \end{bmatrix} & . & . & 0 \\ . & . & . & . & . \\ 0 & . & . & . & \begin{bmatrix} \sigma_{18} & \omega_{18} \\ -\omega_{18} & \sigma_{18} \end{bmatrix} \end{bmatrix} \tag{5}$$

where Λ is a 4×4 matrix containing the eigenvalues corresponding to the rigid-body modes:

$$\Lambda = \begin{bmatrix} \lambda_1 & 0 & 0 & 0 \\ 0 & \lambda_2 & 0 & 0 \\ 0 & 0 & \sigma_p & \omega_p \\ 0 & 0 & -\omega_p & \sigma_p \end{bmatrix} \tag{6}$$

λ_1, λ_2 denote the two real eigenvalues corresponding to the short period mode, and σ_p, ω_p denote the real and imaginary parts of the eigenvalues corresponding to the phugoid-like mode. σ_i, ω_i , $i = 1, 2, ...18$, denote the real and imaginary parts of the eigenvalue

corresponding to the ith flexible mode. After these transformations, the B and C matrices no longer have the forms shown previously. However, the transfer function can now be expressed in the parallel form, i.e., as the sum of transfer functions corresponding to individual modes, which facilitates model order reduction.

$$P(s) = P_r(s) + \sum_{i=1}^{i=18} P_i(s) \tag{7}$$

where $P_r(s)$ and $P_i(s)$ denote the (2×1) transfer functions corresponding to the rigid-body modes and the ith flexible mode, respectively.

The simplest method of order reduction would be to truncate all flexible modes beyond a certain frequency. However, this approach does not generally yield favorable results because some of the higher frequency modes may be prominent. Balanced realization [3], which represents a better method of model reduction, uses a similarity transformation to make the controllability and observability grammians equal and diagonal. Only the k most controllable and observable state variables are retained to obtain a kth order model. Other methods include optimal Hankel norm approximation [4], and stable factorization [5]. However, the application of these methods results in fully coupled system matrices, causing loss of physical insight. An alternate method consists of assessing the controllability and observability of flexible modes (λ_i) by ranking them in the order of the reciprocal condition numbers (evaluated at $s = \lambda_i$) of the matrices $[sI - A \quad B]$ and $[sI - A^T \quad C^T]$ respectively [6]. The most controllable/observable modes are then retained. Another alternate method, which offers considerable physical insight, is to rank the flexible modes in the order of their operator norms (H_2 or H_∞):

$$\|P_i(s)\|_2 = \int_0^\infty Tr[P_i(t)P_i^T(t)]dt \tag{8}$$

where $P_i(t)$ denotes the impulse response matrix of $P_i(s)$, and $Tr[.]$ denotes the trace operator,

$$\|P_i(s)\|_\infty = \sup_{\omega\in(-\infty,\infty)} \overline{\sigma}[P(j\omega)] \tag{9}$$

where $\overline{\sigma}[.]$ denotes the largest singular value. For lightly damped flexible modes, it is well-known (see [7]) that the modal coordinates are approximately balanced and thus nearly uncorrelated.

The H_2 norm basically represents the energy in the impulse response, while the H_∞ norm represents an upper bound on the gain. The 2-norm can be readily obtained by computing the controllability or observability grammian [8], and closed-form expressions can be derived for both the 2-norm and the ∞-norm for the present case.

The contribution of each flexible mode to the overall transfer function was computed using H_2 and H_∞ norms of the transfer function of each mode. The modal rankings (from highest to lowest norms) are given in Table II. There is some agreement between the two rankings, with the exception of mode 4. The H_∞ norm is more appropriate for

order reduction because we use the additive uncertainty robustness test, which employs the upper bound on the H_∞ norm. The two modes with the largest H_∞ norms are modes 1 and 4, which are the 1st free fuselage bending mode and the 2nd cantilevered fuselage bending mode respectively.

4 LQG-Type Controller Design

When a reduced-order design model is used for LQG-type controller design, the closed-loop stability cannot be guaranteed because of control and observation "spillovers" [9], which consist of the inadvertent excitation of the uncontrolled modes by the control input, and the unwanted contribution of the uncontrolled modes to the sensor outputs (See Figure 1). One method of ensuring stability in the presence of spillovers is to represent the uncontrolled mode dynamics as "additive uncertainty" $\Delta P(s)$, which is in parallel with the design model $P_o(s)$ (Figure 2). This formulation has been used extensively in flexible spacecraft control [6], [10]. An upper bound on the magnitude $\overline{\sigma}[\Delta P(j\omega)]$ can be obtained to form an "uncertainty envelope". The height of the uncertainty envelope represents the worst-case damping ratios and mode-shape magnitudes of the uncontrolled modes, while the width accommodates lateral shifts in the peaks due to uncertainties in the natural frequencies. A scalar transfer function $P_u(s)$ can be obtained by inspection of the $\overline{\sigma}[\Delta P(j\omega)]$ plot to represent the uncertainty envelope, so that $\mid P_u(j\omega) \mid \geq \overline{\sigma}[\Delta P(j\omega)]$.

The design model, which consists only of the controlled modes, is given by:

$$\dot{x}_d = A_d x_d + B_d u + v \tag{10}$$

$$y_d = C_d x_d + w \tag{11}$$

where x_d, y_d are the state and output vectors, and v, w denote zero-mean white noise vectors.

The controller design problem can be formulated as an LQG design problem with th e following objective function

$$J = \lim_{t\to\infty} \mathcal{E}[x_d^T(t) Q x_d(t) + u^T(t) R u(t)] \tag{12}$$

where $\mathcal{E}$ denotes the expected value, $Q = Q^T \geq 0$, $R = R^T > 0$. The design parameters are the LQ regulator (LQR) weighting matrices Q and R, as well as the Kalman-Bucy filter (KBF) weighting matrices $V = V^T \geq 0$ and $W = W^T > 0$. (In theory, V and W represent the process noise and sensor noise covariance intensities; however, they are actually used as design parameters to obtain satisfactory controller response).

A sufficient condition for stability in the presence of unstructured additive uncertainty is [8]:

$$\overline{\sigma}[\Delta P C (I + P_0 C)^{-1}] < 1 \ \forall \ real \ \omega \tag{13}$$

where $C(s)$ denotes the controller transfer function matrix, and the argument $(j\omega)$ has been dropped for convenience. The following two conditions are also sufficient:

$$\overline{\sigma}[\Delta P] < \frac{1}{\overline{\sigma}[C(I+P_0C)^{-1}]} \; \forall \; real \; \omega \tag{14}$$

$$\mid P_u \mid < \frac{1}{\overline{\sigma}[C(I+P_0C)^{-1}]} \; \forall \; real \; \omega \tag{15}$$

The control objectives are to stabilize the unstable rigid mode, and to obtain a crisp pitch-angle step response to elevator step input. In addition the controller must be robust to unmodeled aeroelastic modes, and if possible, should increase the damping of the aeroelastic modes that are included in the design model. The design process, which has been used in the past for flexible spacecraft control [6], is summarized as follows:

1. Select design parameters Q, R, V, W to obtain a nominal LQG controller for the design model, that gives satisfactory closed-loop eigenvalues and frequency response.

2. Apply the robustness test in the presence of additive uncertainty. If the test fails, adjust the weighting matrices and go back to step 1.

3. Repeat until satisfactory performance and robustness are obtained.

(A systematic procedure, based on an analytical expression for H_∞-norm sensitivity, was presented in [11] for reducing the left-hand term in Eq. (13). This procedure can be used to perform Step 2). Two different controller designs were performed. The first (4th-order) controller was based on a design model consisting only of the four rigid-body state variables, with all the flexible modes lumped into an "additive uncertainty". The second (8th-order) controller consisted of the rigid-body states and the four state variables corresponding to two most significant flexible modes.

4.1 Fourth-Order Controller

In this case, A_d is equal to Λ, and B_d and C_d are defined accordingly. Figure 3 shows the singular value plot (or σ-plot) of the flexible mode transfer function containing all 18 flexible modes. The following scalar transfer function, whose magnitude plot "envelopes" the uncertainty, was obtained by trial and error: (See Figure 3):

$$P_u(s) = \frac{100(s+0.5)^2}{(s+2)(s+5)(s+10)} \tag{16}$$

While attempting a nominal LQG controller design, it was found to be difficult to increase the closed-loop frequency of the phugoid-like mode while simultaneously moving the unstable short period mode deeper into the left half plane. Despite several trials, it was not possible to find LQR weights which gave suitable pole locations. However, it was

known that a proportional plus integral (PI) control law developed in [2] gave satisfactory closed-loop pole locations. Therefore, an inverse LQR problem was formulated and solved, which gave the corresponding Q matrix (with $R = 1$) for the "rigid-only" design model. (A discussion of the inverse LQR problem can be found in [12]). The set of closed-loop poles of the design model, which is the union of the LQR and KBF poles, governs the closed-loop system's speed of response (bandwidth). Therefore the initial V and W were chosen to obtain closed-loop pole KBF pole locations close to those for the LQR.

The initial LQG controller failed to satisfy the robustness condition of Eq. (15), and it was necessary to reduce the controller gain by reducing appropriate elements of Q and V. After a few iterations involving weight adjustments for the LQR and the KBF, the robustness condition was satisfied (Figure 4). The controller, whose frequency response is shown in Figure 5, is unstable, although the closed-loop system is stable and robust to unmodeled flexible modes. The closed-loop LQR and KBF eigenvalues are shown in Table III, and the closed-loop eigenvalues of the complete 40th-order system are given in Table IV. The phugoid-like mode's closed-loop frequency (for both LQR and KBF) shows substantial improvement as compared to the open-loop value. There is no significant change in the flexible mode frequencies and damping ratios. This controller, although robust to unmodeled flexible modes, was found to give a poor response to step input in the elevator. In particular, it had a 136 % overshoot and a settling time of nearly 150 sec. (We define settling time as the time beyond which the step response remains within 10 % of its final value). In order to improve the controller, the LQR weighting function was modified by the addition of the term $c.\theta^2$, where c is a constant. It was found that only small performance improvement was possible without violating the robustness test (15).

4.2 Eighth-order Controller

In order to improve the rigid-body response and the flexible mode damping, an eighth order design model was next considered, which consists of four rigid-body states and four state variables corresponding to flexible modes 1 and 4, which have the largest ∞-norms. Figure 6 shows the σ-plot of modes 1 and 4 only, as compared to the σ-plot of all 18 flexible modes. It can be seen that modes 1 and 4 capture the highest peaks of the complete flexible dynamics. The σ-plot for the remaining elastic modes 2, 3, and 5-18, is shown in Figure 7. The system matrix for the 8th-order design model is given by:

$$A_d = diag[\Lambda, \begin{bmatrix} \sigma_1 & \omega_1 \\ -\omega_1 & \sigma_1 \end{bmatrix}, \begin{bmatrix} \sigma_4 & \omega_4 \\ -\omega_4 & \sigma_4 \end{bmatrix}] \tag{17}$$

For this model, the following $P_u(s)$ was chosen as the uncertainty envelope:

$$P_u(s) = \frac{200(s+1)}{(s+20)(s+80)} \tag{18}$$

To obtain the 8×8 Q matrix for the design model, the 4×4 Q matrix used in the initial iteration of the 4th-order controller design was augmented by adding weights corresponding to the flexible mode states. The weights in the second 4×4 diagonal block of Q were adjusted to increase the flexible mode damping and frequencies. R was held at unity. The KBF weights were selected to obtain closed-loop estimator eigenvalues with magnitudes roughly equal to those for the LQR. The initial controller did not satisfy the additive uncertainty robustness condition; hence iterative loop shaping was performed until the condition was satisfied. For this case, it was possible to increase the phugoid-like mode's closed-loop frequency to 0.85 rad/sec (for LQR) and 0.7 rad/sec (for KBF), which represents nearly 100 percent improvement over the 4th-order controller. In addition, the (LQR and KBF) damping ratios for flexible mode 1 increased to over 0.1 as compared to its open-loop value of 0.07. The damping ratio for mode 4 increased to 0.076 for the LQR and 0.041 for the KBF, as compared to its open-loop value of 0.014. The LQR and KBF eigenvalues are given in Table V. The closed-loop eigenvalues of the complete (40th-order) evaluation model are given in Table VI. The closed-loop eigenvalues are somewhat different from the LQR and KBF eigenvalues, but still indicate significantly superior performance than the 4th-order controller. Figure 8 shows the final additive uncertainty robustness test. The controller frequency response is shown in Figure 9. As in the case of the 4th-order controller, the 8th-order controller $C(s)$ is itself unstable, although the closed-loop system is stable as well as robust to unmodeled flexible modes. The response to a step input in the elevator was significantly better than that of the 4th-order controller. Figures 10 and 11 show the (normalized) pitch angle and rate at gyro location 1 resulting from a step input in the elevator. The settling time is nearly 100 sec. and the overshoot is 36 %. It was not possible to significantly improve the response without violating the condition in (15). The effect of the flexible modes is seen in the pitch rate response (Figure 11). The improvement in the damping (for modes 1 and 4) was rather small, and any attempts to further improve the damping by increasing the weights resulted in the violation of the robustness condition. The results indicate that it is difficult to improve aeroelastic mode damping using the elevator as the only input.

5 Robustness to Parametric Uncertainties

The controllers designed in the previous section offer robust stability in the presence of unmodeled flexible modes. Furthermore, uncertainties in the unmodeled dynamics are tolerated without instability as long as the magnitude plot $\overline{\sigma}[\Delta P(j\omega)]$ lies below the uncertainty envelope $\mid P_u(j\omega) \mid$. However, the designs assume perfect knowledge of the design model parameters, which may also have significant uncertainties. Therefore it is important to investigate the robustness of the controllers in the presence of parametric uncertainties in the design model.

Robustness to structured parametric uncertainties can be investigated using the structured singular value (or $\mu-$) analysis [13]. The problem with standard $\mu-$analysis is that it assumes the uncertainties to be complex-valued rather than real which usually results in overly conservative estimates of permissible parametric uncertainty. The development of $\mu-$analysis and synthesis methods for real parametric uncertainties continues to be an active area of research.

Alternative approaches for the estimation of permissible parametric uncertainty include Kharitonov methods and Lyapunov methods. A fundamental result by Kharitonov (see [14]) addresses polynomials with uncertain coefficients which lie in given intervals, and gives a necessary and sufficient condition for the roots to be in the open left-half plane (OLHP). In practice, however, the mapping from the parameter space to the characteristic polynomial coefficients is not only highly nonlinear and often intractable, but also results in the coefficients being inter-related. As a result, the robustness conditions are usually quite conservative.

Lyapunov-based methods essentially obtain norm bounds on the perturbation in the closed-loop system matrices, while utilizing the information about the structure of the uncertainty to the maximum extent possible. Consider the system;

$$\dot{x} = (A_o + E)x := Ax \tag{19}$$

where A_o is the nominal system matrix and E is the perturbation matrix. A_o is assumed to be stable (as would be the case if a nominal stabilizing control law is used). Suppose each element E_{ij} is bounded in an interval:

$$\mid E_{ij} \mid \leq \epsilon_{ij} \tag{20}$$

Let

$$\epsilon = \max_{i,j} \epsilon_{ij} \tag{21}$$

Define the matrix U_e as follows:

$$U_{e_{ij}} = \frac{\epsilon_{ij}}{\epsilon} \tag{22}$$

That is, U_e denotes the "relative error" matrix. All the elements of U_e are positive. Suppose $Q = Q^T > 0$ is an $n \times n$ matrix and P is the symmetric positive positive definite solution of the Lyapunov equation;

$$A_o^T P + P A_o = -Q \tag{23}$$

Let P_m denote the "modulus matrix" of P:

$$P_{m_{ij}} = \mid P_{ij} \mid \tag{24}$$

Let $[.]_s$ denote the symmetric part of a matrix L, i.e.,

$$L_s = \frac{1}{2}(L + L^T) \tag{25}$$

The following sufficient conditions are based on Lyapunov methods.

Condition 1- (Patel and Toda, 1980 [15]): The perturbed system is stable for all $\mid E_{ij} \mid \leq \epsilon_{ij}$ if

$$\overline{\sigma}(E) < \frac{\lambda_m(Q)}{2\lambda_M(P)} \tag{26}$$

where $\lambda_m(.)$ and $\lambda_M(.)$ denote the smallest and largest eigenvalues.

If E is as in Eq. (20), $E_m = \epsilon\, U_e$, and

$$\overline{\sigma}(E) \leq \overline{\sigma}(E_m) = \epsilon\, \overline{\sigma}(U_e) \tag{27}$$

Then a sufficient condition for stability is:

$$\epsilon < \frac{\lambda_m(Q)}{2\overline{\sigma}(U_e)\lambda_M(P)} \tag{28}$$

If all the parameters are equally perturbed, $\mid E_{ij} \mid = \epsilon$, and $\overline{\sigma}(U_e) = n$.

Condition 2- (Yedavalli, 1985 [16]): The perturbed system is stable if

$$\epsilon < \frac{\lambda_m(Q)}{2\lambda_M[(P_m U_e)_s]} \tag{29}$$

5.1 Robustness of Dynamic Compensator

Consider the m-input, l-output, nth order system:

$$\dot{x} = (A_o + \Delta A)x + (B_o + \Delta B)u \tag{30}$$

$$y = (C_o + \Delta C)x \tag{31}$$

where $\Delta A,\ \Delta B,\ \Delta C$ denote the perturbations in the nominal system matrices (A_o, B_o, C_o). Suppose the system is controlled by an n_cth order dynamic controller:

$$\dot{x}_c = A_c x_c + B_c y \tag{32}$$

$$u = -C_c x_c \tag{33}$$

Denoting $\overline{x} = (x^T, x_c^T)^T$, the $\overline{n}$th order ($\overline{n} = n + n_c$) closed-loop system can be written as:

$$\dot{\overline{x}} = (\overline{A}_o + \overline{E})\overline{x} \tag{34}$$

where

$$\overline{A}_o = \begin{bmatrix} A_o & -B_o C_c \\ B_c C_o & A_c \end{bmatrix} \quad \overline{E} = \begin{bmatrix} \Delta A & -\Delta B C_c \\ B_c \Delta C & 0 \end{bmatrix} \tag{35}$$

Let

$$\mid \Delta A_{ij} \mid \leq \epsilon_{A_{ij}}, \quad \mid \Delta B_{ij} \mid \leq \epsilon_{B_{ij}}, \quad \mid \Delta C_{ij} \mid \leq \epsilon_{C_{ij}} \tag{36}$$

The upper bound ϵ_{ij} on E_{ij} is obtained as follows:

$$For\ i,j \in [1,n],\ \epsilon_{ij} = \epsilon_{A_{ij}} \tag{37}$$

$$For\ i \in [1,n],\ j \in [n+1,\overline{n}],\ \epsilon_{ij} = \max_{\substack{i\in[1,n]\\ j\in[n+1,\overline{n}]}} \sum_{k=1}^{m} \Delta B_{ik} C_{c_{kj}} = \sum_{k=1}^{m} \epsilon_{B_{ik}} \mid C_{c_{kj}} \mid \tag{38}$$

$$For\ i \in [n+1,\overline{n}],\ j \in [1,n],\ \epsilon_{ij} = \max_{\substack{i\in[n+1,\overline{n}]\\ j\in[1,n]}} \sum_{k=1}^{l} B_{c_{ik}} \Delta C_{kj} = \sum_{k=1}^{l} \epsilon_{C_{kj}} \mid B_{c_{ik}} \mid \tag{39}$$

$$For\ i,j \in [n+1,\overline{n}],\ \ \epsilon_{ij} = 0 \tag{40}$$

Then ϵ and U_e can be defined as in Eqs. (21), (22).

Suppose $\overline{P}$ and $\overline{Q}$ are positive definite symmetric matrices such that

$$\overline{A}_o^T \overline{P} + \overline{P}\overline{A}_o = -\overline{Q} \tag{41}$$

The conditions (26) and (29) can be used to obtain the robustness bound on ϵ. The sufficient condition of (29) is generally less conservative than that of (26). It should be noted, however, that both bounds depend on the choice of the $\overline{Q}$ matrix. At present there appear to be no systematic methods available for choosing $\overline{Q}$.

If the dynamic compensator is an LQG-type controller designed for the nominal plant (A_o, B_o, C_o), it can be easily verified that

$$A_c = A_o - B_o G - H C_o \tag{42}$$

$$B_c = H \tag{43}$$

$$C_c = G \tag{44}$$

where G and H denote the LQR and KBF gain matrices respectively.

5.2 Robustness Results for the SCRA Model

The Lyapunov-based sufficient conditions were used to investigate robustness of the 8th-order LQG controller to parametric uncertainties in the design model. Based on experience with flexible space structures [6], the parametric uncertainties most important for stability robustness are those in the flexible mode frequencies. Therefore the uncertainties in the frequencies (ω_1 *and* ω_4) of the two flexible modes included in the design model were investigated. Since no systematic methods exist for choosing $\overline{Q}$, the value $\overline{Q} = 2I$ was used in (41), and the allowable bounds on frequency perturbations were obtained from conditions 1 and 2. The maximum permissible perturbation (in both ω_1 and ω_4) obtained using Condition 1 was 6.9×10^{-3} percent, while that obtained using Condition 2 was 0.93 percent, which indicates that Condition 2 is far less conservative than Condition 1.

The frequency domain additive uncertainty condition (14) was next used to investigate the permissible perturbation bounds in ω_1 and ω_4. For this case, ω_1 and ω_4 in the 40th-order plant ($P(s)$) were perturbed by certain percentages, and the additive uncertainty $\Delta P(s)$ [$= P(s) - P_o(s)$] consisted of both parametric uncertainties and unmodeled flexible modes. Figure 12 shows the robustness condition for 3 percent perturbation in ω_1 and 2 percent perturbation in ω_4. The condition was violated for larger perturbations. Based on these results, the 8th-order controller can tolerate ± 3 percent uncertainty in ω_1 and ± 2 percent uncertainty in ω_4. These bounds are better than the Lyapunov-based bounds despite the fact that the latter utilize the information about the structure of the uncertainty. To investigate the degree of conservatism of the frequency-domain bounds, the eigenvalues of the complete 48th-order closed-loop system were computed for a large number (about 300) of combinations of perturbed values of ω_1 and ω_4. The closed-loop system remained stable well beyond the permissible bounds indicated by the frequency domain condition. In particular, perturbations of well over 30 percent in ω_1 and ω_4 were tolerated without instability, which indicates that the 8th-order controller has good robustness to these uncertainties.

The results obtained indicate that Lyapunov-based methods generally yielded conservative bounds for permissible parametric uncertainty, as compared to the frequency domain unstructured uncertainty formulation. It should be noted, however, that the Lyapunov bounds were obtained with an arbitrary choice of the $\overline{Q}$ matrix, and therefore a general conclusion cannot be drawn regarding the conservatism of the methods. It may be possible to improve the Lyapunov bounds by optimally choosing $\overline{Q}$ to maximize the bound. The bounds, however, are not differentiable; therefore, conventional gradient-based optimization methods cannot be readily applied. Additional results were recently reported in [17] in this area, which can yield less conservative Lyapunov-based bounds, and they should be investigated.

6 Concluding Remarks

Controller design was considered for longitudinal control of a supersonic transport aircraft model in the presence of significant aeroelastic modes. Two controllers were designed using frequency domain loop shaping employing the LQG method, wherein the unmodeled flexible modes were represented as additive uncertainty. The first (4th-order) controller was designed to control only the rigid-body modes without destabilizing the flexible modes, while the second (8th-order) controller was designed to control the rigid-body modes and the two most prominent flexible modes. The 4th-order controller gave poor performance characterized by excessive overshoot and large settling time. It was not possible to improve the 4th-order design while still guaranteeing stability in the presence of unmodeled flexible modes. The 8th-order controller gave significantly better performance, which indicates the necessity of including some of the aeroelastic modes in the design model for controller

design for this class of aircraft. It was not possible to substantially improve the flexible mode damping ratios without destabilizing the uncontrolled modes. Based on the design iterations performed, it appears to be difficult- if not impossible- to obtain higher performance with only one actuator and two sensors. The robustness of the 8th-order controller to uncertainties in the flexible mode frequencies was investigated using Lyapunov-based methods as well as frequency domain tests. The Lyapunov-based methods gave more conservative bounds on the permissible parametric uncertainty as compared to the frequency domain unstructured uncertainty formulation. The latter method, which itself is conservative, indicated rather small uncertainty tolerance in flexible mode frequencies. Numerical experimentation, however, demonstrated that the controller can tolerate over 30 % uncertainty in the flexible mode frequencies without instability. The results indicate that further research is needed on methods for robust control design and damping enhancement for such systems. It would also be highly desirable to investigate methods for reducing the conservatism of the Lyapunov-based robustness bounds.

References

[1] Ashkenas, I. L., Magdaleno, R. E., and McRuer, D. T.: Flight Control and Analysis Methods for Studying Flying and Ride Qualities of Flexible Transport Aircraft. NASA CR 172201, August 1983.

[2] Newman, B., and Buttrill, C.: Conventional Flight Control for an Aeroelastic Relaxed Static Stability High-Speed Transport. Paper AIAA-95-3250-CP, Proc. AIAA GN&C Conference, Aug. 1995, Baltimore, MD, pp. 717-726.

[3] Moore, B. C.: Principal Component Analysis in Linear Systems: Controllability, Observability, and Model Reduction. *IEEE Trans. Auto. Contr.*, Vol. AC-26, No. 1, Feb. 1981, pp. 17-32.

[4] Glover, K.: All Optimal Hankel Norm Approximations for Linear Multivariable Systems and Their L_∞-Error Bounds. *International J. Control*, Vol. 39, No. 6, 1984, pp. 1115-1193.

[5] Vidyasagar, M.: *Control Systems Synthesis: A Factorization Approach.* Cambridge, MA: MIT Press, 1985.

[6] Joshi, S. M.: *Control of Large Flexible Space Structures.* Vol. 131, Lecture Notes in Control and Information Sciences, Berlin: Springer-Verlag, 1989.

[7] Gawronski, W., and Williams, T.: Model Reduction for Flexible Space Structures. *J. Guidance, Control, and Dynamics*, Vol. 14, No. 1, Jan.-Feb. 1991, pp.68-76.

[8] Green, M., and Limebeer, D. J.: *Linear Robust Control*, N.J.: Prentice-Hall, 1995.

[9] Balas, M. J.: Trends in Large Space Structures Control Theory: Fondest Hopes, Wildest Dreams. *IEEE Trans. Auto. Contr.*, Vol. AC-27, No. 3, June 1982, pp. 522-535.

[10] Lim, K. B., Maghami, P. G., and Joshi, S. M.: Comparison of Controller Designs for an Experimental Flexible Structure. *IEEE Control Systems Magazine*, Vol. 12, No. 3, June 1992, pp. 108-118.

[11] Giesy, D. P., and Lim, K. B.: H_∞ Norm Sensitivity Formula with Control System Design Application. *J. Guidance, Control, and Dynamics*, Vol. 16, No. 6, Nov.-Dec. 1993, pp.1138-1145.

[12] Anderson, B. D. O., and Moore, J. B.: *Optimal Control: Linear Quadratic Methods*, N.J.: Prentice Hall, 1990.

[13] Maciejowski, J. M.: *Multivariable Feedback Design*, Workingham, U.K.: Addison-Wesley, 1989.

[14] Barmish, B. R.: New Tools for Robustness Analysis, *Recent Advances in Robust Control*, P. Dorato and R. K. Yedavalli, Eds., N.Y.: IEEE Press, 1990, pp. 5-10.

[15] Patel, R. V., and Toda, M.: Quantitative Measures of Robustness for Multivariable Systems. Paper TP8-A, Proc. 1980 Joint Automatic Control Conference, San Francisco, 1980.

[16] Yedavalli, R. K.: Perturbation Bounds for Robust Stability in Linear State Space Models. *International J. Control*, Vol. 42, No. 6, 1985, pp. 1507-1517.

[17] Yedavalli, R. K.: Flight Control Application of New Stability Robustness Bounds for Linear Uncertain Systems. *J. Guidance, Control, and Dynamics*, Vol. 16, No. 6, Nov.-Dec. 1993, pp. 1032-1037.

Table I. Open-loop eigenvalues

Elastic mode no.	Eigenvalue	Frequency	Damping ratio
Rigid	0.1024	0.1024	-1.0000
	-0.1347±0.1093i	0.1735	0.7763
	-1.2131	1.2131	1.0000
1	-0.4810±6.6284i	6.6458	0.0724
2	-1.9879±11.5569i	11.7267	0.1695
3	-1.4348±14.7948i	14.8642	0.0965
4	-0.2287±16.4597i	16.4613	0.0139
5	-0.6289±23.3865i	23.3949	0.0269
6	-0.6680±26.0988i	26.1074	0.0256
7	-1.9759±28.6077i	28.6758	0.0689
8	-0.5698±30.2615i	30.2668	0.0188
9	-0.7014±32.1394i	32.1471	0.0218
10	-2.1891±34.0663i	34.1365	0.0641
11	-0.9042±35.6527i	35.6642	0.0254
12	-1.0329±37.6960i	37.7102	0.0274
13	-2.0194±40.0825i	40.1334	0.0503
14	-0.9870±42.3950i	42.4065	0.0233
15	-1.1167±44.0393i	44.0535	0.0253
16	-0.9666±45.2971i	45.3074	0.0213
17	-2.7348±46.5604i	46.6406	0.0586
18	-1.0438±47.2865i	47.2980	0.0221

Table II. Norm ranking of elastic modes in descending order

H_2 - norm :	1, 13, 12, 3, 14, 4, 9, 10, 15, 6, 16, 18, 17, 8, 2, 11, 5, 7
H_∞ - norm :	1, 4, 12, 13, 3, 14, 9, 6, 15, 10, 16, 18, 8, 5, 11, 2, 17, 7

Table III. Regulator and estimator eigenvalues for 4th order controller

Eigenvalue	Frequency	Damping ratio
LQ R eigenvalues		
-0.0180	0.0180	1.0000
-0.3204±0.2886i	0.4312	0.7430
-1.2071	1.2071	1.0000
KBF eigenvalues		
-0.1024	0.1024	1.0000
-0.3089±0.2234i	0.3812	0.8102
-1.2131	1.2131	1.0000

Table IV. Closed-loop eigenvalues for 4th order controller

	Eigenvalue	Frequency	Damping ratio
Rigid	-0.0199	0.0199	1.0000
	-0.1004	0.1004	1.0000
	-0.2850±0.1872i	0.3410	0.8358
	-0.2974±0.3595i	0.4666	0.6374
	-1.2081	1.2081	1.0000
	-1.2131	1.2131	1.0000
Elastic	-0.5222±6.8813i	6.9011	0.0757
	-1.9893±11.5629i	11.7328	0.1696
	-1.4302±14.7344i	14.8036	0.0966
	-0.2391±16.4538i	16.4556	0.0145
	-0.6293±23.3853i	23.3938	0.0269
	-0.6697±26.0918i	26.1004	0.0257
	-1.9733±28.6090i	28.6770	0.0688
	-0.5686±30.2592i	30.2645	0.0188
	-0.7075±32.1268i	32.1346	0.0220
	-2.1835±34.0534i	34.1233	0.0640
	-0.9054±35.6541i	35.6656	0.0254
	-1.0404±37.6805i	37.6948	0.0276
	-2.0124±40.0627i	40.1133	0.0502
	-0.9858±42.3963i	42.4078	0.0232
	-1.1155±44.0343i	44.0484	0.0253
	-0.9666±45.2994i	45.3097	0.0213
	-2.7355±46.5600i	46.6403	0.0587
	-1.0429±47.2865i	47.2980	0.0220

Table V. Regulator and estimator eigenvalues for 8th order controller

	Eigenvalue	Frequency	Damping ratio
	LQ R eigenvalues		
Rigid	-0.0083	0.0083	1.0000
	-0.6484±0.5533i	0.8524	0.7607
	-1.1348	1.1348	1.0000
Elastic	-0.9283±6.5950i	6.6600	0.1394
	-1.2317±16.4513i	16.4973	0.0747
	KBF eigenvalues		
Rigid	-0.1024	0.1024	1.0000
	-0.6963±0.0907i	0.7022	0.9916
	-1.2131	1.2131	1.0000
Elastic	-0.6679±6.6133i	6.6469	0.1005
	-0.6715±16.4568i	16.4705	0.0408

Table VI. Closed-loop eigenvalues for 8th order controller

	Eigenvalue	Frequency	Damping ratio
Rigid	-0.0108	0.0108	1.0000
	-0.0997	0.0997	1.0000
	-0.5680	0.5680	1.0000
	-0.5607±0.5043i	0.7542	0.7435
	-1.1562±0.1742i	1.1692	0.9888
	-1.2131	1.2131	1.0000
Elastic	-0.6587±6.6122i	6.6449	0.0991
	-0.9951±6.5730i	6.6479	0.1497
	-2.0533±11.6470i	11.8266	0.1736
	-0.8210±14.0037i	14.0277	0.0585
	-0.4396±16.4927i	16.4985	0.0266
	-2.0118±16.7903i	16.9104	0.1190
	-0.6252±23.3700i	23.3783	0.0267
	-0.6943±26.0593i	26.0686	0.0266
	-1.9551±28.6190i	28.6857	0.0682
	-0.5588±30.2423i	30.2474	0.0185
	-0.7284±32.0308i	32.0391	0.0227
	-2.1631±34.0027i	34.0714	0.0635
	-0.9177±35.6657i	35.6775	0.0257
	-1.0781±37.5127i	37.5282	0.0287
	-1.8832±39.8877i	39.9321	0.0472
	-0.9495±42.3830i	42.3936	0.0224
	-1.1040±43.9945i	44.0083	0.0251
	-0.9646±45.3059i	45.3162	0.0213
	-2.7393±46.5498i	46.6304	0.0587
	-1.0309±47.2873i	47.2985	0.0218

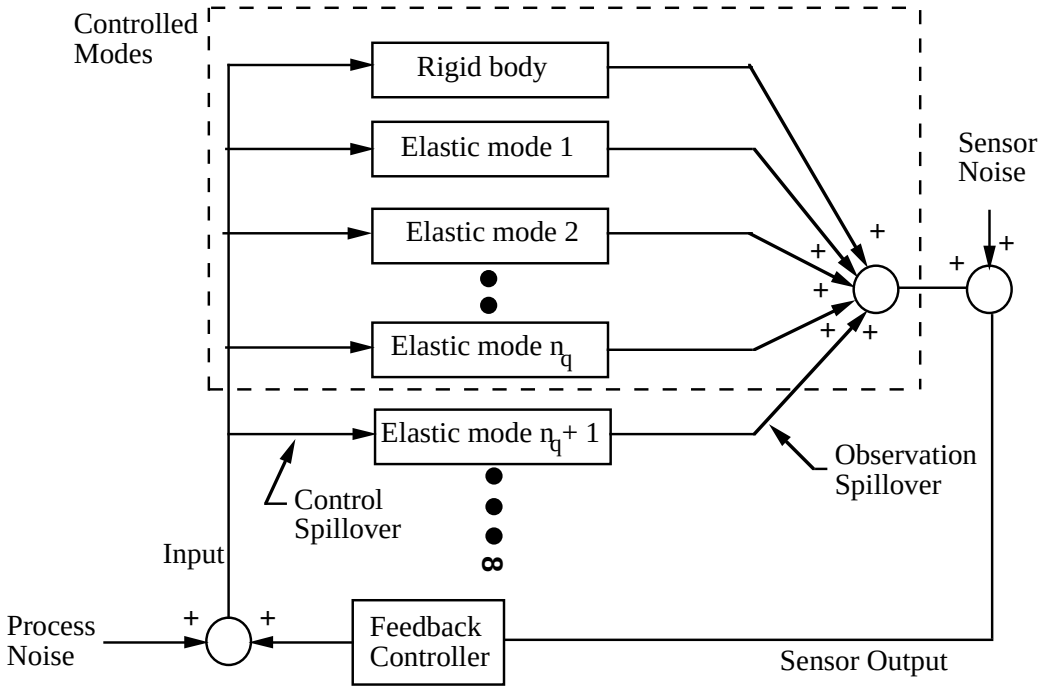

Figure 1: Control and observation spillover

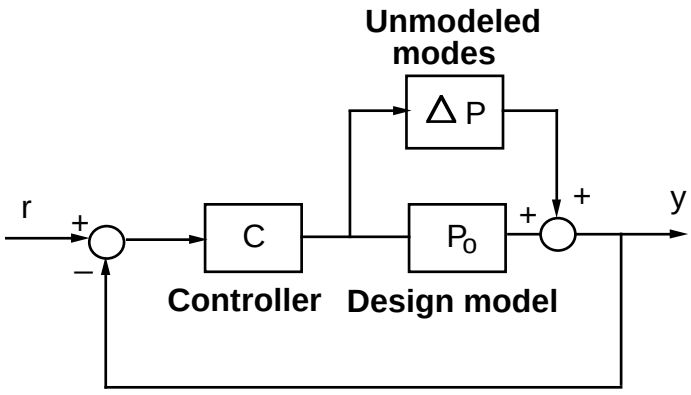

Figure 2: Additive uncertainty formulation

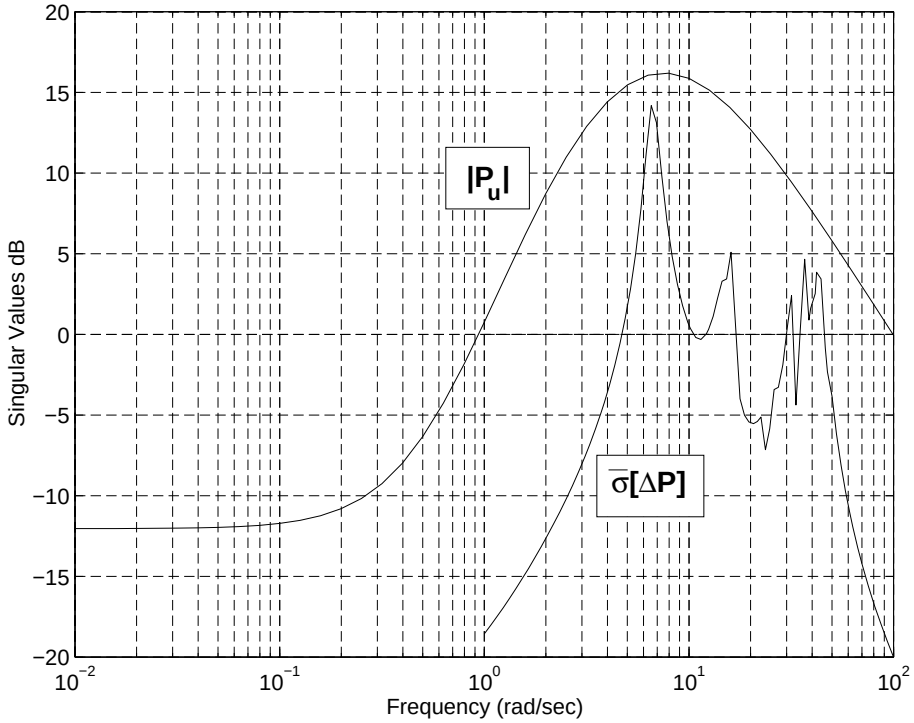

Figure 3: Uncertainty envelope for 4th-order controller

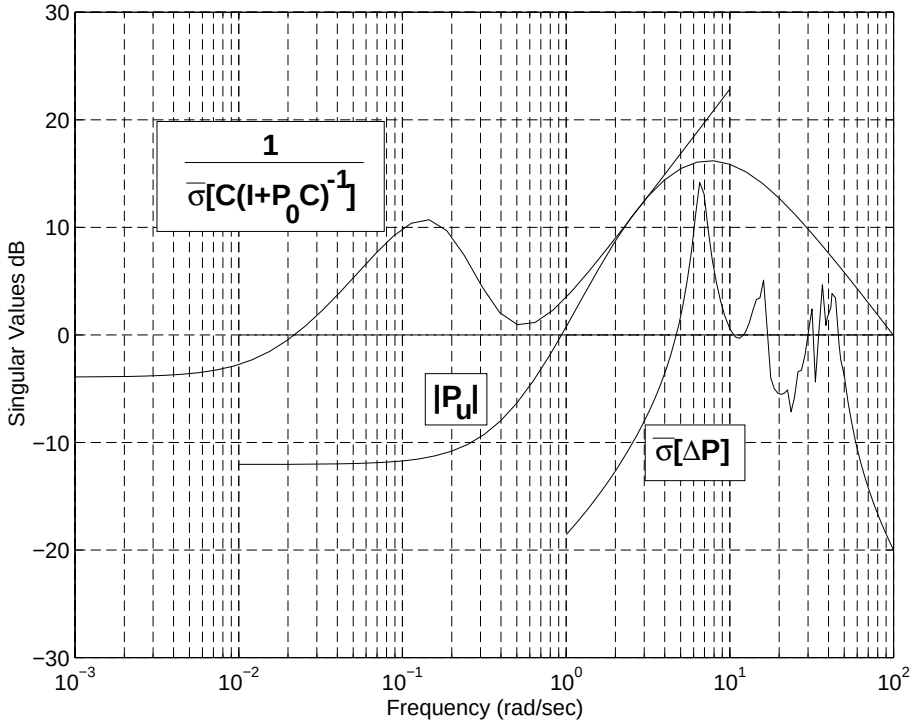

Figure 4: Robustness test for 4th-order controller

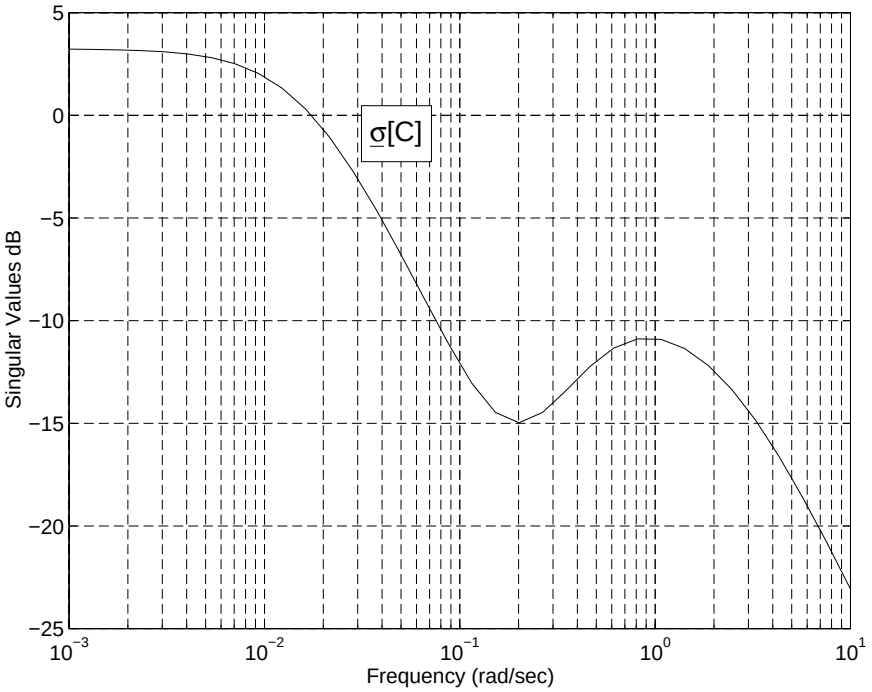

Figure 5: Frequency response of 4th-order controller

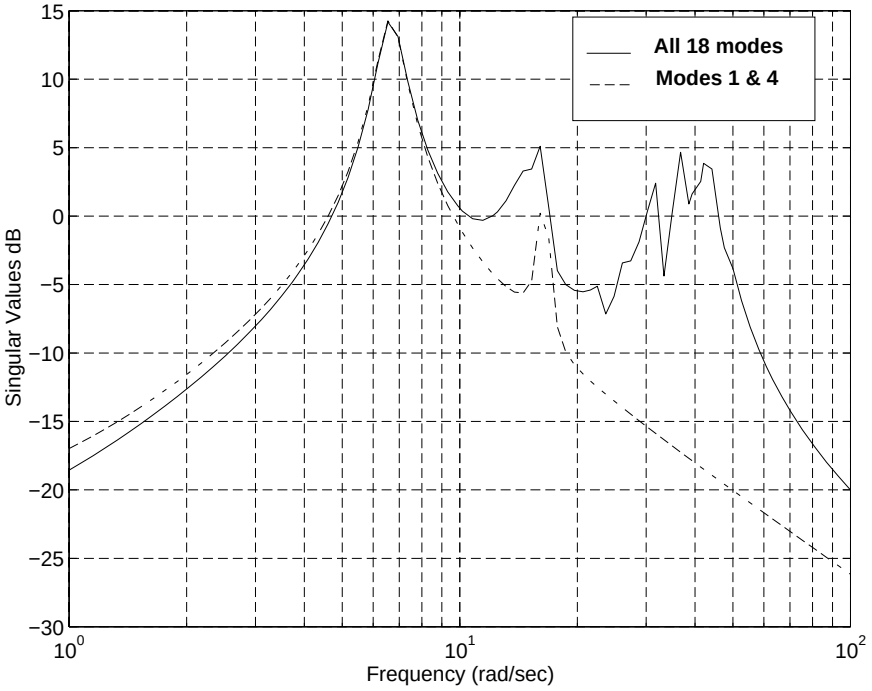

Figure 6: σ-plot of flexible modes

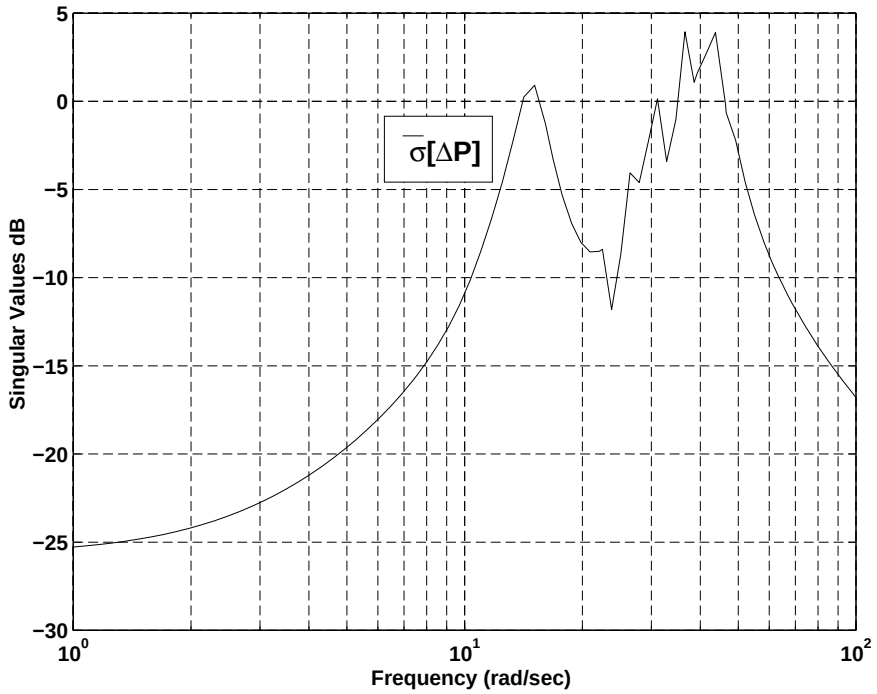

Figure 7: σ-plot of modes 2,3, and 5-18

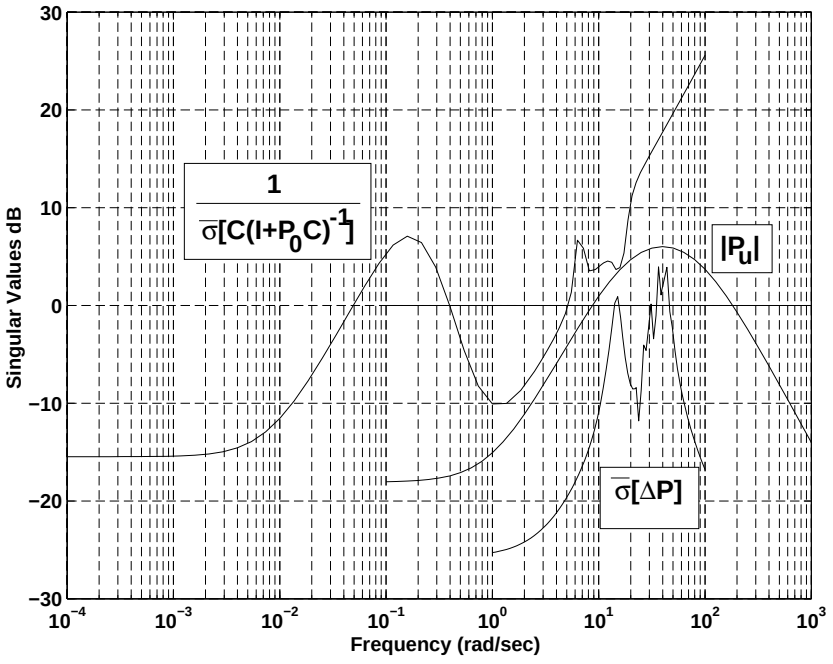

Figure 8: Robustness test for 8th-order controller

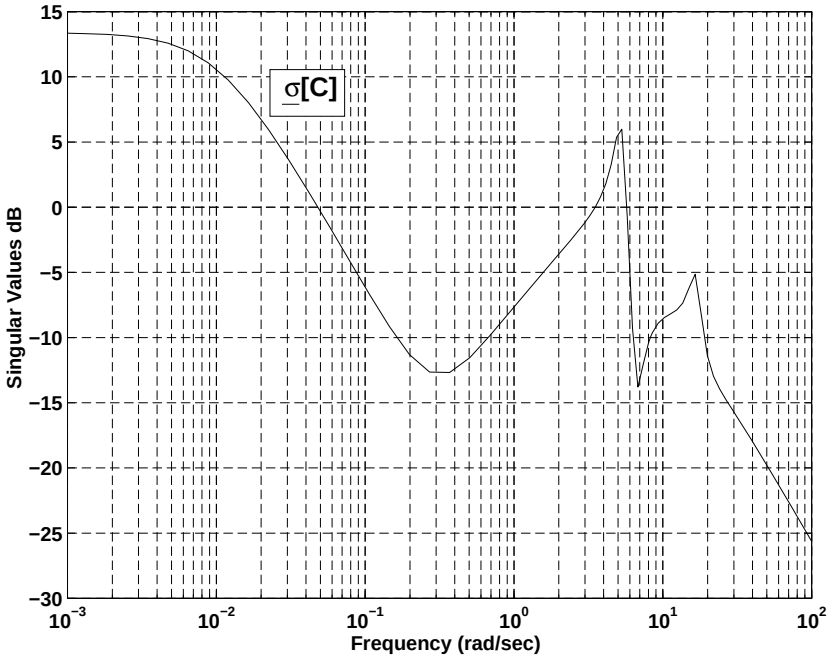

Figure 9: Frequency response of 8th-order controller

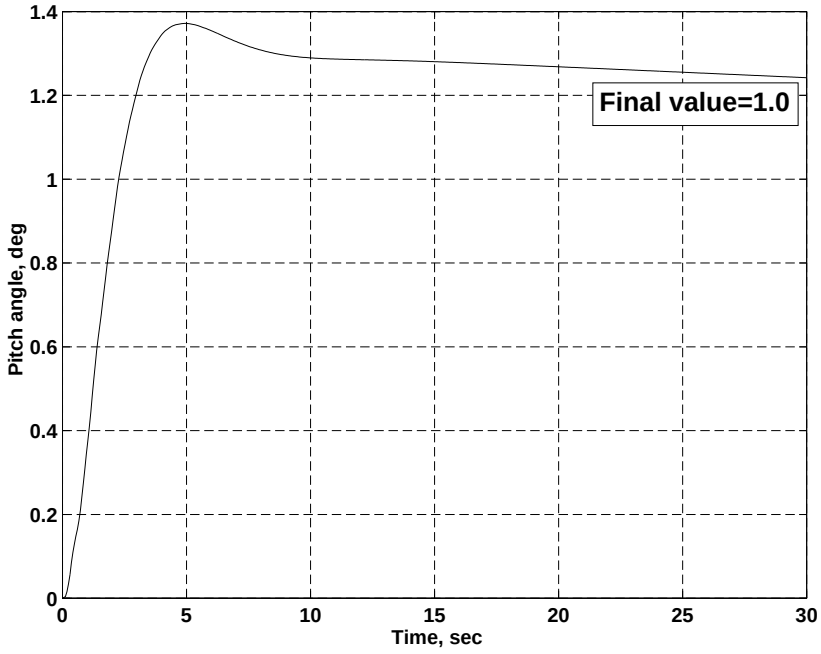

Figure 10: Step response (pitch angle at gyro 1)

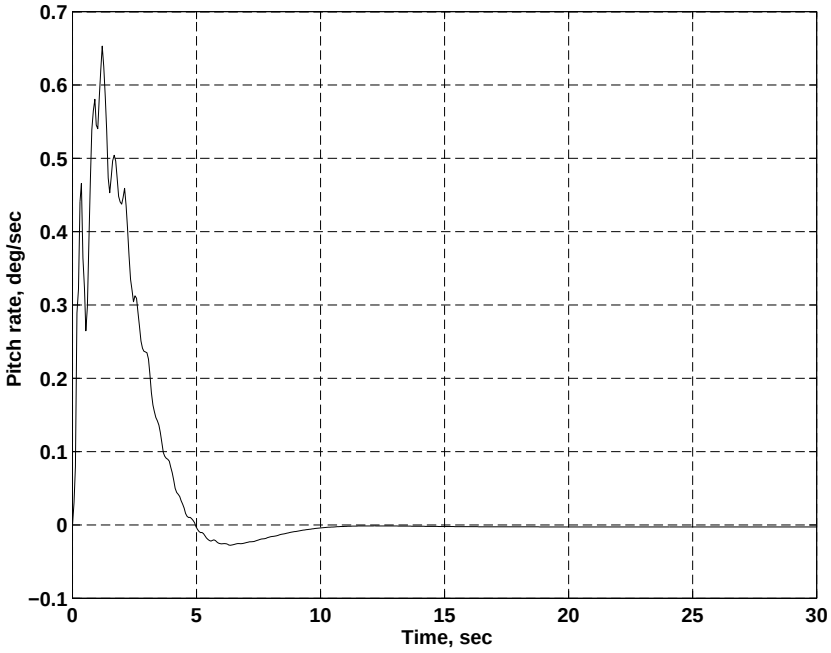

Figure 11: Step response (pitch rate at gyro 1)

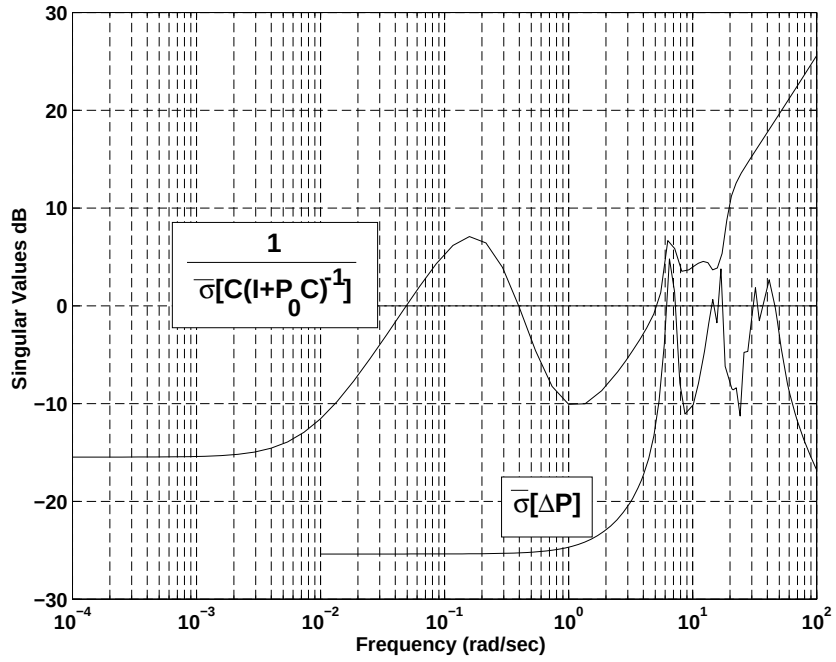

Figure 12: Robustness test in the presence of uncertainty in ω_1 and ω_4